Tunable optical properties of silicon-on-insulator photonic crystal slab structures

A. C. Tasolamprou
atasolam@auth.gr
Department of Electrical and Computer Engineering, Aristotle University of Thessaloniki, Thessaloniki GR-54124, Greece

B. Bellini
Consiglio Nazionale delle Ricerche, Istituto per la Microelettronica e Microsistemi (CNR-IMM), via del fosso del cavaliere 100, 00133, Rome, Italy

D. C. Zografopoulos
Department of Electrical and Computer Engineering, Aristotle University of Thessaloniki, Thessaloniki GR-54124, Greece

E. E. Kriezis
Department of Electrical and Computer Engineering, Aristotle University of Thessaloniki, Thessaloniki GR-54124, Greece

R. Beccherelli
romeo.beccherelli@artov.imm.cnr.it
Consiglio Nazionale delle Ricerche, Istituto per la Microelettronica e Microsistemi (CNR-IMM), via del fosso del cavaliere 100, 00133, Rome, Italy

A photonic crystal slab structure with one-dimensional periodicity, obtained by preferential etching of a silicon-on-insulator wafer, is numerically investigated in 3-D. The etched grooves are considered to be filled either with an isotropic or with a Nematic Liquid Crystal (NLC) material. The molecular director is calculated using a consistent model of NLC reorientation under an external voltage. Different structures together with a broad range of voltage values are numerically simulated by means of a three-dimensional finite-difference time-domain method. The shifting of the photonic bandgap induced by the applied voltage, as well as its sensitivity in terms of refractometric applications, are discussed for a range of different structure geometries. [DOI: 10.2971/jeos.2009.09017]

Keywords: photonic crystals, liquid crystals, silicon-on-insulator

1 INTRODUCTION

Photonic Crystals (PhCs) are periodic optical structures in one, two or three dimensions and due to their property of prohibiting light transmission inside a certain range of wavelengths they have attracted continually growing attention in the field of sensing systems and communications [1]. For the design and fabrication of PhCs several materials such as semiconductors [2], metals [3] and magnetic materials [4] have been proposed over the last years. Among these materials the Silicon-On-Insulator (SOI) heterostructure appears to be promising. It provides strong optical confinement due to the high index contrast between silicon and SiO_2, it is a relatively low cost material, and moreover it is compatible with CMOS technology [5]. Indeed, SOI based nanophotonics technology has demonstrated significant progress in recent years [6]–[9]. A variety of submicron-scale devices, proven to be beneficial in terms of sensitivity and compactness, has been so far produced. In addition, the achievement of light emission on silicon substrate, as well as the trend to set up a library of photonic functions, have consolidated the domain of silicon photonics [10, 11]. As far as the fabrication of nanostructures is concerned, several different technologies such as electron beam lithography (e.g. [12]), deep UV lithography [13] and nano-imprinting [14] have been developed. Our approach consists in exploiting the very high selectivity of anisotropic etching on monocrystalline silicon, which is a process that naturally leads to very smooth sidewalls and well-controlled geometries. Based on this principle the design and fabrication of micro-metre scale optical devices filled with polymers and Liquid Crystals (LCs) is presented in [15] and the experimental characterisation of the nematic liquid crystal channel waveguide is reported in [16]. Scaling down this fabrication method, we have designed slanted PhCs on SOI and studied their infiltration by a Liquid Crystal (LC). The presence of the LC in the device is expected to boost it with electrically tunable properties at low power consumption [17].

A preliminary theoretical study investigating the optical properties of the corresponding 2D geometry [18] showed that a bandgap effectively appears in such a structure. It has also been described how the bandgap is modified by reorienting the LC infiltrated in the grooves. This structure has thus appeared promising in terms of fabrication simplicity, hence cost-effectiveness, and LC integration and control. A more complete and realistic understanding of the structure requires a consistent, fully vectorial, three dimensional modelling of the electro-optical behaviour of the LC-infiltrated PhC. In this paper, after a brief description of the structure in Section 2, Section 3 will present the optical behaviour of a PhC infiltrated with an isotropic material. Emphasis will be put on the influence of the grating width. Further to this, we will consider the case of LC infiltration and analyse the subsequent electro-optical behaviour.

Received March 09, 2009; published April 13, 2009 ISSN 1990-2573

2 DESCRIPTION OF THE STRUCTURE

The 3D structure under investigation is shown in Figure 1. It is implemented on a SOI substrate, characterized by a top silicon layer of 220 nm thickness and followed by a silica buried dioxide (BOX) layer of thickness h_{sub}. The BOX layer extends upon a bulk silicon layer (not shown in Figure 1), which is considered to be conductive (highly doped). The optical input waveguide is a silicon rib of width $W_1 = 450$ nm; the width has been chosen in order to ensure single-mode propagation for the given height of the waveguide at the wavelength of 1.55 μm. After propagation, light is collected at the exit of the device by the optical output waveguide of W_3 width, as shown in Figure 1. It is assumed that the exit waveguide can smoothly regain its initial width W_1, which permits single-mode propagation, via an adiabatic taper transition.

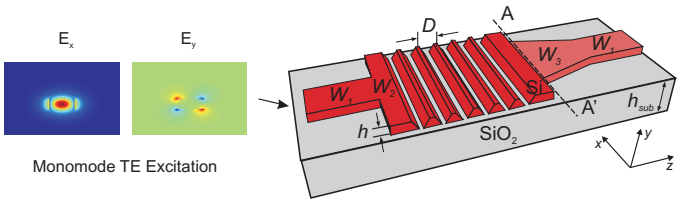

FIG. 1 Schematic layout of the three dimensional grooved photonic crystal rib waveguide.

The main part of the device, which is responsible for the optical properties studied in the present work, is the PhC itself, otherwise termed as the grating region. With respect to the input waveguide, the width of the PhC section is enlarged to $W_2 > W_1$. This region typically involves a small number of periods of trapezoidal grooves, six in the context of the present study. The bottom and top bases equal to 370 nm and 50 nm, respectively, producing a structure with a photonic crystal period of $D = 420$ nm. The grooves are etched by anisotropic preferential etching, using an alkaline solution as reported in [18, 19]. The refractive indices of Si and SiO_2 for the wavelengths here studied (1.3 μm $< \lambda <$ 2.3 μm) are considered to be 3.5 and 1.45, respectively. We assume that the grooves are infiltrated either with an isotropic fluid of index n_i or with a nematic LC of a birefringence $\Delta n = 0.38$ (ordinary index $n_o = 1.55$, extraordinary index $n_e = 1.93$). Finally, the cover is an ITO-deposited glass plate of refractive index 1.45, which allows the application of an external electric field between cover and substrate. The gap between the glass cover and the silicon region is ideally null. However in practice it always has a finite value h_{sup}, due to imperfections of the fabrication process. This gap is assumed to be infiltrated with the same material as in the grooves.

3 STUDY OF THE INFILTRATION OF THE STRUCTURE

The bandgap tuning properties of the structure were investigated numerically in the context of a fully anisotropic 3-D finite-difference time-domain (FDTD) analysis [20]. All nine components of the dielectric tensor calculated within the grooves (see Section 3.2.1) are introduced in a custom FDTD code, while the computational window is terminated by Perfectly Matched Layers (PMLs). The computational substrate extends to 0.5 μm below the Si top layer, while the superstrate extends 1 μm upwards; both regions are terminated by using a PML. The waveguide is excited by the fundamental TE mode supported by a rib waveguide of height $h = 220$ nm and width of $W_1 = 450$ nm (see inset in Figure 1). The transmission spectra are acquired by performing an FFT at the exit of the grating region, before the taper transition (cross-section AA', Figure 1) and are normalized with respect to the transmission of a single mode un-patterned silicon rib waveguide of constant width $W_1 = W_2 = 450$ nm and equal length. The optical structure analysis is initially focused on the case where the etched area is filled with an isotropic material invariant to any external tuning and further when the grooves are infiltrated with a highly birefringent NLC under the application of the external electrical field.

3.1 Infiltration with an isotropic material

3.1.1 Effect of W_2

The first approach to the evaluation of the optical properties of the 3D structure refers to the case where an isotropic material infiltrates the grooves. To begin with, the impact on the bandgap formation in the infiltrated structure is examined with respect to the variation of the value of the etched area's width W_2. The overlayer is assumed thick enough, so that $h_{sup} = +\infty$.

Figure 2 demonstrates the transmission curves assessed for a structure whose grooves as well as the whole region of the superstrate are considered to be infiltrated with an isotropic material of refractive index equal to 1.5, for different values of W_2 ranging from 450 nm to 1200 nm. The reference dashed curve corresponds to a structure of infinite W_1 and W_2, similar to the case of the two dimensional structures studied in [18] and here it has been calculated by artificially imposing periodic conditions along the x-axis in the 3D simulation.

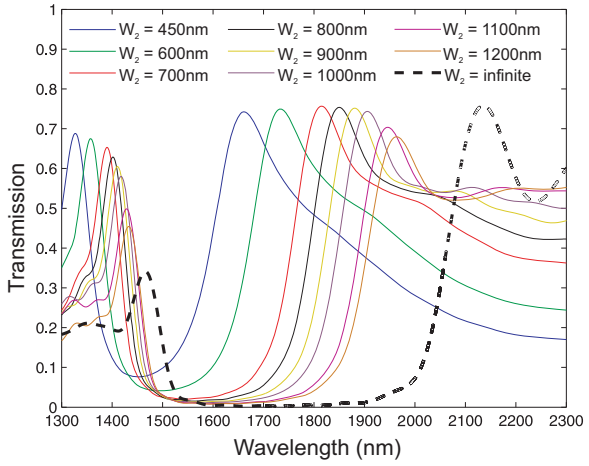

FIG. 2 Transmission curves calculated for a structure corresponding to grooves infiltrated by an isotropic material ($n = 1.5$), for different values of $W_2 = 450$ nm, 600 nm, 700 nm, 800 nm, 900 nm, 1000 nm, 1100 nm, 1200 nm. The width W_1 is kept fixed at 450 nm. The dashed curve corresponds to the case of the two dimensional structure (W_1 and W_2 are infinite, groove and superstrate index equal to 1.5).

The results are indicative of the bandgap properties of the structure in terms of the variation of the transverse dimension of the main area of propagation in the waveguide. It

is observed that for the case where the width of the rib remains invariant ($W_2 = W_1 = 450$ nm) the bandgap (blue curve) is quite narrow and not very well defined. However, as the etched region becomes successively wider the bandgap broadens and the edges are becoming more clearly defined. Moreover the structure tends to qualitatively imitate the optical behaviour of the infinite W_2 reference case, although a direct comparison should also take into account the different excitation between the 3-D and the 2-D structure.

3.1.2 Effect of refractive index

Next we consider the case of a grating section of $W_2 = 1000$ nm and a finite overlayer h_{sup}. The grooves as well as the overlayer are considered to be infiltrated with an isotropic material of various values of refractive index, while the rest of the superstrate region is glass ($n = 1.5$). Figure 3 demonstrates the family of transmission curves corresponding to a filling material of refractive index varying from $n = 1.3$ to $n = 1.9$ with a step of 0.1, when $h_{sup} = 200$ nm. It can be noticed that the high-frequency band edge is much more sensitive to the index change than the low-frequency band edge. As a result, the bandgap shrinks when increasing the refractive index.

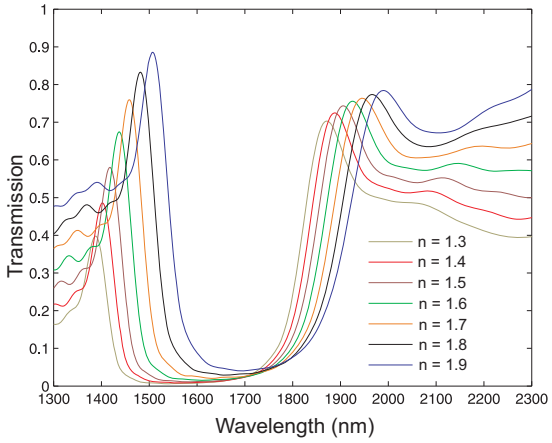

FIG. 3 Transmission curves calculated for a structure of fixed width $W_2 = 1000$ nm. The grooves and the overlayer of $h_{sup} = 200$ nm are infiltrated by an isotropic material of refractive index n ranging from 1.3 to 1.9.

3.1.3 Refractometric applications

Further insight in the optical properties of the structure is provided by investigating its sensing capability, in the context of designing a compact refractometric device, where the unknown liquid is assumed to infiltrate the grooves of the periodic structure. Similarly to Figure 3 the family of transmission curves for the infiltration with an isotropic material of refractive index varying between $n = 1.3$ and $n = 1.9$ for three values of $W_2 = 750$ nm, 1000 nm and 1200 nm and an overlayer of $h_{sup} = 200$ nm, is demonstrated. For each different structure the testing wavelength chosen is the one where the maximum transmission takes place: $\lambda = 1472$ nm, $\lambda = 1508$ nm and $\lambda = 1526$ nm, correspondingly for each structure. All three maxima occur as expected in the case where the structure is infiltrated with the material of the highest refractive index ($n = 1.9$), while there appears to be a shifting of the maxima with respect to the width W_2 of the structure, towards the lower frequencies in accordance to Figure 2. Figure 4(b) demonstrates the normalized transmission for each case at the above maximum transmission wavelengths as a function of the refractive index. The transmitted power is higher in the case of the narrowest structure, while in all cases the normalized transmission appears to increase exponentially with respect to the infiltrated material index. Calculating the sensitivity as defined in [21], Figure 4(b) (inset) demonstrates the performance of the structure as a sensing device for different choices of the width W_2. It is observed that the structure of the widest $W_2 = 1200$ nm, apart from providing a sharper and wider bandgap, exhibits a more efficient performance as a sensor.

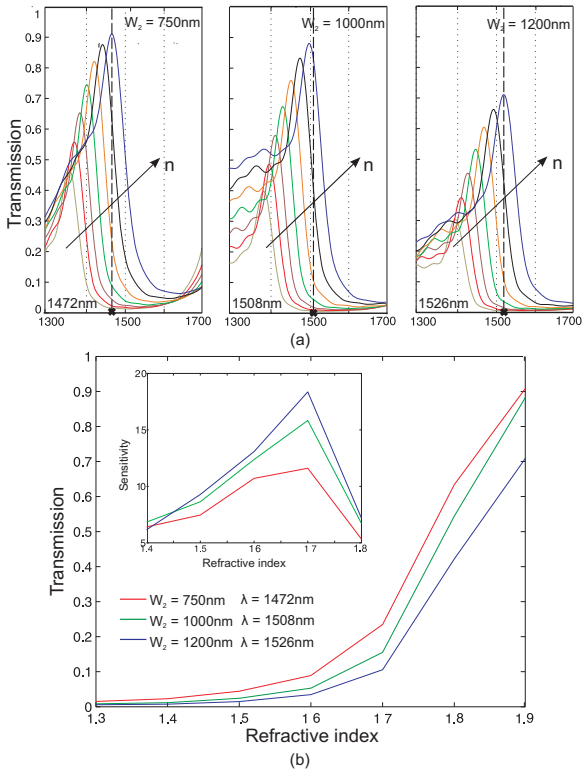

FIG. 4 (a) Transmission curves calculated for a structure corresponding to grooves infiltrated by an isotropic material of refractive index $n = 41.3$ to 1.9 in steps of 0.1, for $W_2 = 750$ nm, 1000 nm, and 1200 nm. The overlayer is $h_{sup} = 200$ nm, and (b) Transmission as a function of refractive index for $W_2 = 750$ nm, 1000 nm, and 1200 nm and (inset) dependance of the sensitivity over the refractive index n.

3.2 Infiltration with a Nematic LC

3.2.1 LC director tuning

Tunable optical properties are achieved in the case where the etched grooves are considered to be infiltrated by a highly-birefringent NLC material. The optical properties of this material can be altered under the dynamic control of external parameters, here by applying an electric field perpendicularly to the substrate.

In order to predict the behaviour and performance of the LC infiltrated photonic crystal structure, it is necessary to calculate the response of the nematic material to the application of the external field. The LC director's configuration is evaluated via the finite-element method (FEM), based on the weak form approach to simplify the highly nonlinear iteration equation [22]. The calculations were performed by taking into account

the coupling between the electrostatic problem and the minimization of the Oseen-Frank free elastic energy [23] over the material's bulk. The static permittivity of the LC is characterized by a parallel component of $\epsilon_{\parallel} = 20$ and a perpendicular of $\epsilon_{\perp} = 7$, while its elastic constants K_{11}, K_{22} and K_{33} are equal to 6.4 pN, 4 pN and 10 pN respectively.

The electric field responsible for the optical tuning is considered to be applied between an ITO electrode placed above the residual LC layer and the bottom bulk silicon layer which is assumed to be a perfect conductor. Thus at the top of the conductor a voltage V is applied, while the bottom of the conductor is kept grounded and there are no density charges in the edges of the grooves. At the Si/LC boundary as well as at the top surface homogeneous strong anchoring conditions are assumed, while periodic conditions are applied at the sidewalls. The molecules that are adjacent both to the groove's walls and the top surface are considered to lie parallel to the groove's axis. This boundary condition depends on the interaction between the LC molecules and the considered surface and in order to impose it, an alignment layer is often used (generally rubbed or photoaligned polymer or evaporated SiOx). Slanted grooves permit the deposition of this layer. In the absence of electric field, the nematic director is everywhere parallel to the groove's axis and the tilt and twist angles equal zero. Nevertheless, in the present simulations of the director's profile, in order to achieve satisfactory convergence a small pre-tilt and pre-twist angle of 2° is assumed. The application of the electric field reorientates the LC molecules and leads to the formation of a director pattern, characterized locally by the tilt and the twist angles.

As observed in Figure 5 for an indicative set of increasing values of the applied voltage ($V = 10, 40, 120$ V), the tilt angle tends towards 90° in the free bulk area, while remaining more restricted close to the surfaces. Above a saturating value of the voltage further tuning of the director is no longer possible. A more detailed prediction of the behaviour of the tilt angle of the material is presented in Figure 5(a) where the average tilt angle is calculated along the y axis, in the middle of the structure, for various values of the applied voltage. In the residual layer when a voltage close to the saturating value is applied the average tilt angle θ_{av} is almost equal to the maximum value (90°) and it is obvious that tilting in this area is more efficient than in the grooved region where the LC molecules are restricted by the anchoring conditions. For this structure where the substrate extends to 500 nm and h_{sup} equals to 200 nm (Figure 6) the saturating value of the voltage can be estimated approximately equal to 150 V, as observed in Figure 5(a). Beyond this voltage no significant further switching of the material has been observed. The value of the saturating voltage is related to the thickness of the substrate, and it becomes lower as the substrate becomes thinner. Nevertheless as shown in Figure 5, even under the application of more moderate voltages (40 V) the tilting of the director almost reaches the 70% of its fully switched state.

It should be stressed that the discontinuity observed in Figure 5(a) at the point where the residual layer begins should not be perceived as a discontinuity in the physical problem of the LC tilting, but as simply a product of the abrupt change in the number of the values participating in the averaging of the tilt angle due to the geometry of the structure.

3.2.2 Band-edge electric tuning

In order to predict the optical behaviour of the structure after the infiltration of the grooves with the nematic material and under the application of the external field, the evaluation of the optical tensor from the tilt and twist angle is required.

In the following the 3D optical tensor is derived by extruding the 2D director data as calculated in Section 3.2.1 on the $y-z$ cross-section along the x axis of the grooves (Figure 6). Although via this approximation the exact behaviour of the liquid crystal in the side edges of the grooved region is ignored and edge effects are not taken into account, it has been considered an efficient choice; such phenomena take place locally and far away from the central guiding region, therefore they are not expected to severely influence the waveguiding properties of the structure.

In accordance with the isotropic case the computational substrate extends to 0.5 μm, the superstrate to 1 μm, while the

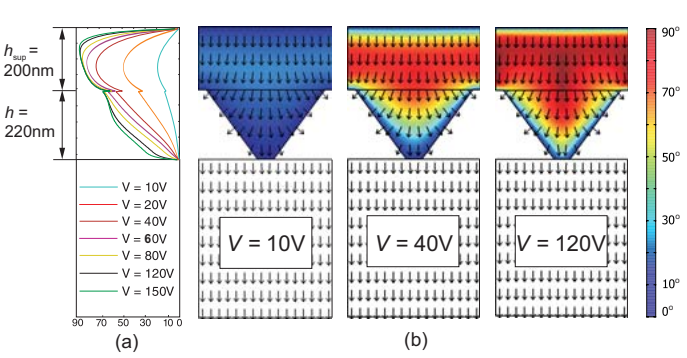

FIG. 5 Nematic director tuning in a single trapezoidal groove etched in silicon: (a) average tilt angle along the y axis, in the middle of the structure, and (b) impact on the tilt angle under the application of a voltage equal to 10 V, 40 V and 120 V. Arrows show the electric field lines.

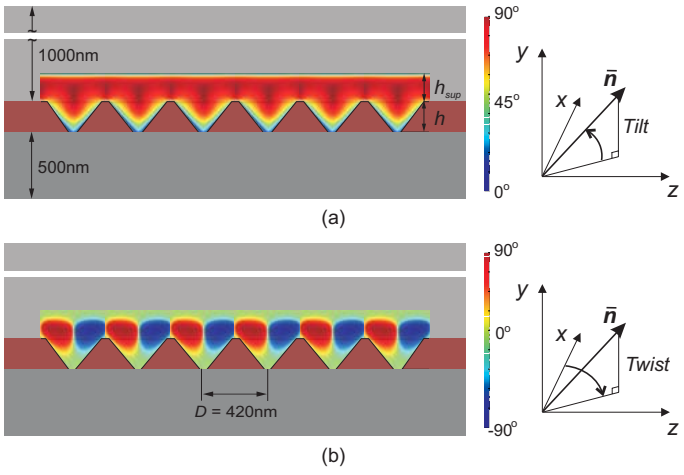

FIG. 6 $y-z$ cross section of the structure demonstrated in Figure 1. The director calculated in Section 3.2.1 for a single groove is repeated for all six grooves and extruded along the x axis, resulting in the formation of the (a) tilt and (b) twist pattern.

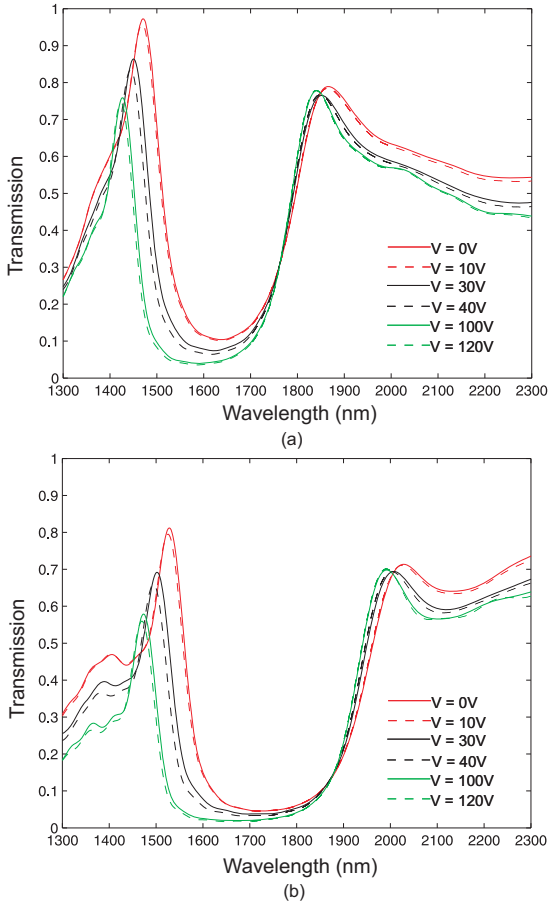

FIG. 7 Transmission curves calculated for a structure corresponding to LC- infiltrated grooves ($n_o = 1.55$, $n_e = 1.93$), superstrate index $n_s = 1.5$, for applied voltages V = 0, 10, 30, 40, 100, 120 V and width (a) $W_2 = 750$ nm and (b) $W_2 = 1200$ nm.

residual layer h_{sup} equals to 200 nm. The NLC infiltrating the grooves is characterized by extraordinary and ordinary indices of $n_e = 1.93$ and $n_o = 1.55$, respectively. The cover is assumed to be glass ($n_s = 1.5$).

Figure 7 shows the bandgaps for different values of the applied voltage for rib waveguide width values of $W_2 = 750$ nm (Figure 7(a)) and $W_2 = 1200$ nm (Figure 7(b)). For small values of the electric field, the TE polarized light perceives the LC almost as an isotropic material of refractive index equal to the extraordinary index of the LC, since all the molecules lie along the groove's axis. As the field grows larger, the LC material in the groove undergoes a threshold transition and is further switched, leading to a considerable broadening of the bandgap. When the applied field reaches the value $V = 120$ V, the molecules of the LC are fully switched and the material in the grooves acts almost as an isotropic material of effective refractive index equal to the ordinary index of the LC.

Taking a closer look at the transmission curves one can observe that when the value of voltage rises from 0 to 120 V the high frequency bandgap edge shifts approximately by $\Delta\lambda$ = 65 nm in the case of the waveguide of $W_2 = 750$ nm width and $\Delta\lambda$ = 85 nm in the case of $W_2 = 1200$ nm width. In both examples the low frequency edge shift remains practically unchanged.

Similarly to Figure 4(b), an evaluation of the normalized transmission with respect to the applied voltage for the anisotropic case is presented in Figure 8(a). For each structure of width $W_2 = 750$ nm, $W_2 = 1000$ nm and $W_2 = 1200$ nm the probe wavelength is chosen to be the one where the transmission obtains the maximum value in the high frequency region. It is observed that these wavelengths almost coincide with these of the isotropic case, since as mentioned above in the absence of applied field the LC is analog to an isotropic material of $n = n_e$.

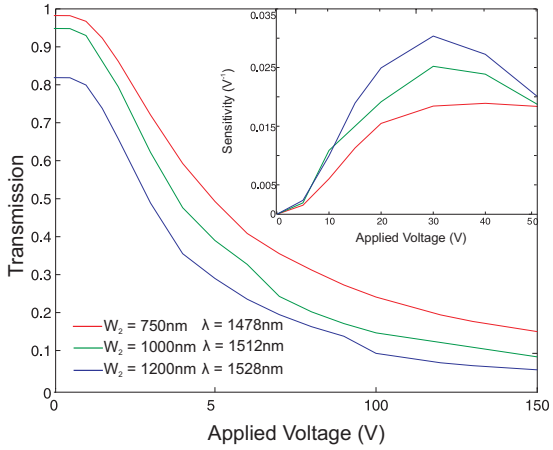

FIG. 8 Normalized transmission as a function of applied voltage for $W_2 = 750$ nm, 1000 nm, and 1200 nm and (inset) dependance of sensitivity over the applied voltage V for $W_2 = 750$ nm, 1000 nm, and 1200 nm.

Once again, it is observed that the narrower the structure the larger the normalized transmission, while for each structure the curves follow an exponential decay with respect to the value of the applied field. In analogy to Section 3.1.3 the sensitivity of the structure with respect to the applied voltage has been studied here. In Figure 8(b), the sensitivity for a structure of $W_2 = 750$ nm, $W_2 = 1000$ nm and $W_2 = 1200$ nm width, under the application of a voltage ranging from 0 to 50 V is demonstrated. It is verified that the structure of width $W_2 = 1200$ nm is more efficient in terms of sensitivity with respect to the applied voltage.

4 CONCLUSIONS

The optical properties of three-dimensional silicon-on-insulator photonic crystal slab structures has been theoretically investigated. Various structures of different geometrical characteristics have been numerically simulated and their optical response with respect to their transverse dimension and the properties of the material infiltrating the etched region have been assessed. The structure has also been studied from the view point of a refractometric optical sensor. Furthermore, its response to an externally applied field in the case of a nematic liquid crystal infiltrating the grooves has been thoroughly studied, based on the calculations of realistic director patterns to the different levels of applied voltage. The corresponding transmission spectra reveal a significant bandgap shift of approximately 85 nm in the air-band in the case where the LC is fully switched. Finally the sensitivity of the structure with respect to a wide range of applied voltage changes has been evaluated.

ACKNOWLEDGEMENTS

The authors acknowledge the financial support of the Italian Ministry of Foreign Affairs.

References

[1] S. Noda, "Recent progresses and future prospects of two- and three-dimensional photonic crystals" J. Lightwave Technol. **24**, 4554–4566 (2006).

[2] P. Pottier, I. Ntakis, and R. M. D. L. Rue, "Photonic crystal continuous taper for low-loss direct coupling into 2D photonic crystal channel waveguides and further device functionality" Opt. Commun. **223**, 339–347 (2003).

[3] P. V. Parimi, W. T. Lu, P. Vodo, J. Sokoloff, J. S. Derov, and S. Sridhar, "Negative Refraction and Left-Handed Electromagnetism in Microwave Photonic Crystals" Phys. Rev. Lett. **92**, 127401 (2004).

[4] C. Z. Fan, G. Wang, and J. P. Huang, "Magnetocontrollable photonic crystals based on colloidal ferrofluids" J. Appl. Phys. **103**, 094107 (2008).

[5] B. Jalali and S. Fathpour, "Silicon photonics" J. Lightwave Technol. **24**, 4600–4615 (2006).

[6] L. Wosinski, M.Dainese, and E. Berglind, *Technology challenges for silicon nanophotonics and beyond* **1**, 183–188 (9th Int. Conf. Transp. Opt. Networks (ICTON07), 2007).

[7] R. T. Chen, *Recent advances in polymer and silicon nanophotonics* 1–25 (Opt. Fiber Comm. / Nat. Fiber Opt. Eng. Conf. (OFC/NFOEC), 2008).

[8] W. Bogaerts, D. Taillaert, B. Luyssaert, P. Dumon, J. V. Campenhout, P. Bienstman, D. V. Thourhout, R. Baets, V. Wiaux, and S. Beckx, "Basic structures for photonic integrated circuits in silicon-on-insulator" Opt. Express **12**, 1583–1591 (2004).

[9] S. P. Chan, V. M. N. Passaro, G. Z. Mashanovich, G. Ensell, and G. T. Reed, "Third order Bragg grating filters in small SOI waveguides" J. Europ. Opt. Soc. Rap. Public. **2**, 07029 (2007).

[10] J. Bruns, T. Mitze, M. Schnarrenberger, L. Zimmermann, M. K. K. Voigt, J. Kreissl, K. Janiak, T. Hartwich, and K. Petermann, "SOI-based optical board technology" Int. J. Electron. Comm. **61**, 158–162 (2007).

[11] G. Roelkens, J. V. Campenhout, J. Brouckaert, D. V. Thourhout, R. Baets, P. R. Romeo, P. Regreny, A. Kazmierczak, C. Seassal, X. Letartre, G. Hollinger, J. Fedeli, L. D. Cioccio, and C. Lagahe-Blanchard, "III-V/Si photonics by die-to-wafer bonding"Materials Today **10**, 36–43 (2007).

[12] B. Schmidt, Q. Xu, J. Shakya, S. Manipatruni, and M. Lipson, "Compact electro-optic modulator on silicon-on-insulator substrates using cavities with ultra-small modal volumes" Opt. Express **15**, 3140–3148 (2007).

[13] W. Bogaerts, V. Wiaux, D. Taillaert, S. Beckx, B. Luyssaert, P. Bienstman, and R. Baets, "Fabrication of photonic crystals in silicon-on-insulator using 248-nm deep UV lithography" IEEE J. Sel. Top. Quant. **8**, 928–934 (2002).

[14] P. I. Borel, B. Bilenberg, L. H. Frandsen, T. Nielsen, J. Fage-Pedersen, A. V. Lavrinenko, J. S. Jensen, O. Sigmund, and A. Kristensen, "Imprinted silicon-based nanophotonics" Opt. Express **15**, 1261–1266 (2007).

[15] B. Bellini, J.-F. Larchanche, J.-P. Vilcot, D. Decoster, R. Beccherelli, and A. d' Alessandro, "Photonic devices based on preferential etching" Appl. Optics **44**, 7181–7186 (2005).

[16] A. d' Alessandro, B. Bellini, R. Beccherelli, D. Donisi, and R. Asquini, "Nematic Liquid Crystal on Silicon Optical Channel Waveguides" IEEE J. Quantum. Elect. **42**, 1084–1090 (2006).

[17] A. D. Falco and G. Assanto, "Tunable wavelength-selective add-drop in liquid crystals on a silicon microresonator" Opt. Commun. **279**, 210–213 (2007).

[18] D. C. Zografopoulos, E. E. Kriezis, B. Bellini, and R. Beccherelli, "Tunable one-dimensional photonic crystal slabs based on preferential etching of silicon" Opt. Express **15**, 1832–1844 (2007).

[19] R. Beccherelli, B. Bellini, D. Zografopoulos, and E. Kriezis, *Tunable one-dimensional photonic crystal slabs* **3**, 6593–15 (Proc. of SPIE Microtechnologies for the New Millennium - Photonic Materials, Devices and Application, 2007).

[20] E. E. Kriezis, C. J. Newton, T. P. Spiller, and S. J. Elston, "Three-dimensional simulations of light propagation in periodic liquid-crystal microstructures" Appl. Optics **41**, 5346–5356 (2002).

[21] W. Hopman, P. Potier, D. Yudistira, J. van Lith, P. Lambeck, R. D. L. Rue, A. Driessen, H. Hoekstra, and R. de Ridder, "Quasi-one-dimensional photonic crystal as a compact building-block for refratometric optical sensors" IEEE J. Sel. Top. Quant. **11**, 11–16 (2005).

[22] J. B. Davies, S. E. Day, F. D. Pasquale, and F. A. Fernandez, "Finite-element modeling in 2-D of nematic liquid crystal structure" Electron. Lett. **32**, 582–583 (1996).

[23] P. de Gennes and J. Prost, *The Physics of Liquid Crystals* (Clarendon Press: Oxford, 1993).